

Josephson systems based on ballistic point contacts between single-band and multi-band superconductors

Y. S. Yerin^{a)}

B. Verkin Institute for Low Temperature Physics and Engineering of the National Academy of Sciences of Ukraine, 47 Lenin Ave., Kharkov 61103, Ukraine and Institute for Physics of Microstructures of the Russian Academy of Sciences, GSP-105, Nizhny Novgorod 603950, Russia

A. S. Kiyko and A. N. Omelyanchouk

B. Verkin Institute for Low Temperature Physics and Engineering of the National Academy of Sciences of Ukraine, 47 Lenin Ave., Kharkov 61103, Ukraine

E. Il'ichev

Leibniz Institute of Photonic Technology, D-07702 Jena, Germany

(Submitted May 13, 2015)

Fiz. Nizk. Temp. **41**, 1133–1147 (November 2015)

The Josephson effect in ballistic point contacts between single-band and multi-band superconductors was investigated. It was found that in the case of Josephson junctions formed by a single-band and an s_{\pm} -wave two-band superconductor as well as by a single-band and a three-band superconductor the junctions become frustrated, showing the φ -contact properties. Depending on the ground state of a three-band superconductor with time-reversal symmetry breaking, the Josephson junction can have from one to three energy minima, some of which can be locally stable. We also study the behavior of a dc SQUID based on the Josephson junctions between single-band and multi-band superconductors. Some features on the dependences of the critical current and the total magnetic flux on the applied flux of a dc SQUID based on the Josephson point contacts between a single-band superconductor and an s_{\pm} -wave superconductor, three-band superconductor with broken time-reversal symmetry and three-band superconductor without broken time-reversal symmetry as compared to the conventional dc SQUIDs based on single-band superconductors were found. The results can be used as an experimental tool to detect the existence of multi-band structure and time-reversal symmetry breaking. © 2015 AIP Publishing LLC. [<http://dx.doi.org/10.1063/1.4935255>]

1. Introduction

One of the most efficient ways of obtaining information about the symmetry of the order parameter in unconventional superconductors is phase-sensitive techniques based on the Josephson effect in such superconducting systems.

Armed with the hypothesis about a possible shape of the Cooper pair wave function, we can theoretically predict specific aspects of the behavior of various Josephson systems based on unusual superconductors. It is these features that form the basis for the techniques known as the Josephson interferometry. This technique involves the study of the magnetic response of a Josephson junction, current-phase relation for the Josephson junctions formed at grain boundaries and SQUID interferometry. Among the variety of the Josephson interferometry techniques, the latter is often the most useful. From a technical point of view, it is based on the study of the characteristics of a one-contact interferometer (a Josephson junction in a superconducting ring) or a dc SQUID (a SQUID ring with two Josephson junctions). In this geometry, one of the superconductors forming the junction has an isotropic s -wave symmetry of the order parameter, while the second one is an unusual superconductor with the symmetry of the order parameter to be revealed.^{1,2}

It is important to note that the Josephson interferometry has already established itself as a useful technique that greatly helped in the identification of d -wave pairing

mechanism of Cooper pairs in cuprate high- T_c superconductors (see, e.g., review Ref. 3).

The recent discovery of a new class of high- T_c superconductors based on iron⁴ gave rise to the question of the pairing mechanism in these compounds and hence the symmetry of the superconducting order parameter. The initially widely accepted hypothesis of the so-called alternating-sign two-component s_{\pm} -wave order parameter^{5,6} does not allow us to unambiguously explain the experimental data for some of the iron superconductors.^{7–14} In this regard, there appeared models based on the assumption of a multi-component chiral structure of the order parameter with the symmetry of the type $s + id$,¹⁵ $s_{\pm} + is_{++}$,¹⁶ or with a conventional s -wave symmetry with three or more gaps. Under certain conditions, the presence of chirality leads to the appearance of frustration, when the time-reversal symmetry in a superconductor is broken.^{17–26} This means that the phases of the order parameter cannot simultaneously satisfy the minimum energy condition, hence creating a two or more fold degenerate ground state.

According to theoretical predictions, time-reversal symmetry breaking in iron superconductors should lead to some interesting phenomena, such as the appearance of spontaneous magnetic field in the presence of nonmagnetic defects, massless Leggett modes and phase solitons (see review Ref. 27 and references therein).

While several technologies have already been proposed for the detection of potential time-reversal symmetry breaking in iron-based superconductors,^{28–31} currently there is no strong experimental evidence for the existence of this phenomenon in iron-based superconductors.

Since the breaking of the time-reversal symmetry is, as a matter of fact, a consequence of the frustration of the order parameter phases, it is logical to assume that for the detection of this phenomenon, the above mentioned phase-sensitive experiments, and in particular the Josephson interferometry, can be advantageous.

Previously, we investigated the Josephson effect³² and the behavior of a dc SQUID containing Josephson point contacts between an *s*-wave superconductor and a three-band isotropic superconductor in the dirty limit.³⁰ We have established the unusual dependence of the critical current on the external magnetic flux and demonstrated the possibility of appearance of multi-hysteresis loops in the dependence of the net flux on the external magnetic flux. It was found that all these features of Josephson systems are associated with time-reversal symmetry breaking. Therefore, the Josephson interferometry is a powerful tool for the detection of this phenomenon. To complete the picture of the possibilities of using the Josephson interferometry to determine the structure of the order parameter and the possible violation of the time-reversal symmetry in iron-based superconductors, in the present paper we will consider the Josephson effect and the behavior of a dc SQUID in another limiting case, when the Josephson point contact between a single-band and a multi-band superconductor exhibits ballistic conduction.

2. Formalism

The theory of the stationary Josephson effect in ballistic point contacts (S-c-S contacts) formed by *s*-wave single-band superconductors has been developed in Ref. 33. The results of this study can be generalized to the point contact between a single-band and an *n*-band ($n \geq 2$) superconductor (Fig. 1).

In this case, the total current flowing through the Josephson junction at any temperature *T* is given by the expression

$$I = \sum_{i=1}^n \frac{2\pi|\Delta_0||\Delta_i|}{eR_{Ni}} \sin(\chi + \phi_i \text{sgn}(i-1)) T \times \sum_{\omega>0} \left\{ \frac{1}{4} \left[\left(\sqrt{\omega^2 + |\Delta_0|^2} + \sqrt{\omega^2 + |\Delta_i|^2} \right)^2 - (|\Delta_0| + |\Delta_i|)^2 \right] + |\Delta_0||\Delta_i| \cos^2 \frac{\chi + \phi_i \text{sgn}(i-1)}{2} \right\}^{-1}. \quad (1)$$

Here, χ is the phase difference between the first order parameters of the *n*-band and the single-band superconductor, $\phi_i = \varphi_i - \varphi_1$ denotes the phase difference between the *i*-th and the first order parameters of the bulk *n*-band superconductor, $|\Delta_0|$ is the magnitude of the energy gap of the single-band superconductor, $|\Delta_i|$ are the magnitudes of the energy gaps of the *n*-band superconductor, ω is the Matsubara frequency, and R_{Ni} are the partial contributions of each band to the total resistance of the contact in the normal state.

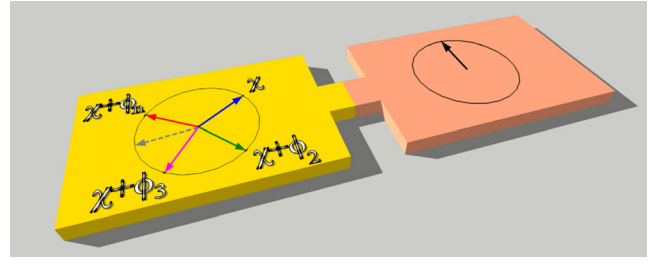


FIG. 1. Schematics of a contact between single-band (coral color) and multi-band (yellow) superconductors. The length of the point contact is much greater than its width, and the width is much smaller than the minimum values of the coherence length and the London penetration depth for the single-band superconductor and the *i*-th band of the multi-band superconductor.

The temperature dependence of the magnitudes of the energy gaps in the *n*-band superconductor can be found by numerical solution of the self-consistency equation

$$|\Delta_i| = 2\pi T \sum_i \sum_j \sum_{\omega>0} \lambda_{ij} \frac{|\Delta_i| \exp[I\phi_i \text{sgn}(i-1)]}{\sqrt{\omega^2 + |\Delta_i|^2}}, \quad (2)$$

where λ_{ij} are the constants of electronic interaction between the bands of the *n*-band superconductor and *I* is the imaginary unit.

Let us make few comments regarding the phase differences ϕ_i , which determine the basic state of an *n*-band superconductor. For a two-band ($n = 2$) clean bulk superconductor, the ground state is non-degenerate with $\varphi_2 = \varphi = 0$ or π , depending on the nature of the interband interaction (attraction or repulsion, respectively). As has been shown in Refs. 31 and 32, in the case of a three-band superconductor, the degeneracy multiplicity of the ground state is determined by the values of the interband interaction coefficients and the modules of the order parameters. In the microscopic description, it has been found that the phase difference of the order parameters $\varphi_2 = \varphi$ and $\varphi_3 = \theta$ can be expressed as:

if $\phi \in [-\frac{\pi}{2}, \frac{\pi}{2}]$ and $\theta \in [-\frac{\pi}{2}, \frac{\pi}{2}]$, then

$$\begin{cases} \phi = \pm \arcsin \Omega, \\ \theta = \mp \arcsin \left(\frac{G_1 |\Delta_2|}{G_3 |\Delta_3|} \Omega \right), \end{cases} \quad \begin{cases} \phi = 0, \\ \theta = 0, \end{cases} \quad (3)$$

if $\phi \in [\frac{\pi}{2}, \frac{3\pi}{2}]$ and $\theta \in [-\frac{\pi}{2}, \frac{\pi}{2}]$, then

$$\begin{cases} \phi = \pi \pm \arcsin \Omega, \\ \theta = \pm \arcsin \left(\frac{G_1 |\Delta_2|}{G_3 |\Delta_3|} \Omega \right), \end{cases} \quad \begin{cases} \phi = \pi, \\ \theta = 0, \end{cases} \quad (4)$$

if $\phi \in [-\frac{\pi}{2}, \frac{\pi}{2}]$ and $\theta \in [\frac{\pi}{2}, \frac{3\pi}{2}]$, then

$$\begin{cases} \phi = \pm \arcsin \Omega, \\ \theta = \pi \pm \arcsin \left(\frac{G_1 |\Delta_2|}{G_3 |\Delta_3|} \Omega \right), \end{cases} \quad \begin{cases} \phi = 0, \\ \theta = \pi, \end{cases} \quad (5)$$

if $\phi \in [\frac{\pi}{2}, \frac{3\pi}{2}]$ and $\theta \in [\frac{\pi}{2}, \frac{3\pi}{2}]$, then

$$\begin{cases} \phi = \pi \pm \arcsin \Omega, \\ \theta = \pi \mp \arcsin \left(\frac{G_1 |\Delta_2|}{G_3 |\Delta_3|} \Omega \right), \end{cases} \quad \begin{cases} \phi = \pi, \\ \theta = \pi. \end{cases} \quad (6)$$

Here

$$\Omega = \sqrt{1 - \left(\frac{G_3^2 G_2^2 |\Delta_3|^2 - G_1^2 G_3^2 |\Delta_1|^2 - G_1^2 G_2^2 |\Delta_2|^2}{2G_1^2 G_2 G_3 |\Delta_1| |\Delta_2|} \right)^2},$$

$G_1 = \lambda_{12}^{-1} N_1 + \lambda_{21}^{-1} N_2$, $G_2 = \lambda_{23}^{-1} N_2 + \lambda_{32}^{-1} N_3$, and $G_3 = \lambda_{13}^{-1} N_1 + \lambda_{31}^{-1} N_3$, where N_i are the densities of states at the Fermi level for each of the bands. The choice of stable solutions, corresponding to the frustrated or non-frustrated states is determined by the second variation of the energy of the three-band superconductor with the difference of the phases φ and θ .

To simplify the analysis of the problem, we make a few assumptions. Let the temperature T be equal to zero and assume that the energy gaps of the superconductors are equal: $|\Delta_0| = |\Delta_i| = |\Delta|$. These assumptions will help to gain qualitative understanding of the main features of the behavior of the Josephson system without resorting to complex numerical solution of Eqs. (2)–(6) in the general case.

Based on these assumptions, from Eq. (1) we obtain an expression for the current flowing through the Josephson junction

$$I = \sum_i \frac{\pi |\Delta|}{e R_{Ni}} \sin \frac{\chi + \phi_i \text{sgn}(i-1)}{2} \text{sgn} \cos \frac{\chi + \phi_i \text{sgn}(i-1)}{2}. \quad (7)$$

Then, by integrating over χ , we find the energy of the Josephson junction

$$E = - \sum_i \frac{\Phi_0 |\Delta|}{2e R_{Ni}} \left| \cos \frac{\chi + \phi_i \text{sgn}(i-1)}{2} \right|. \quad (8)$$

3. Josephson effect in point contacts between single-band and multiband superconductors

As follows from Eqs. (7) and (8), the current flowing through the Josephson junction formed by two single-band s -wave superconductors, is³⁰

$$I = \frac{\pi |\Delta|}{e R_{Ni}} \sin \frac{\chi}{2} \text{sgn} \cos \frac{\chi}{2}, \quad (9)$$

and the energy of the Josephson junction

$$E = - \frac{\Phi_0 |\Delta|}{2e R_{N1}} \left| \cos \frac{\chi}{2} \right|. \quad (10)$$

The current-phase relation for such a contact and the dependence of the Josephson energy on the phase difference is shown in Fig. 2.

It can be seen that the $I(\chi)$ dependence experiences a jump at the point $\chi = \pi$. This jump is the main difference between the Josephson junction with ballistic conductivity and the similar system with diffusive conductivity.³⁴

In the case of a junction formed by single-band and two-band superconductors, the current-phase relation can exhibit new qualitative features if the two-band superconductor has the s_{\pm} -wave symmetry of the order parameter (the characteristics of the Josephson junction with a two-band superconductor of s_{++} -wave symmetry are qualitatively similar to

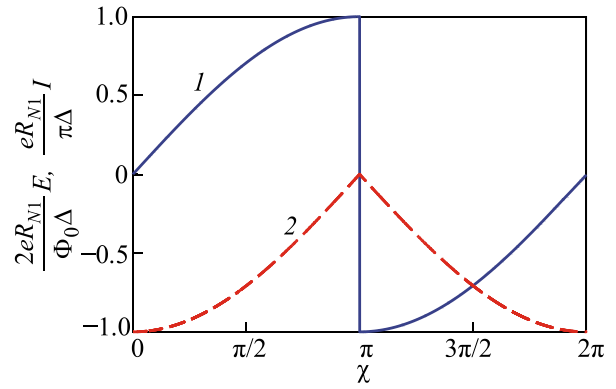


FIG. 2. Current-phase dependence (blue, I) and the Josephson energy (red, 2) of a point contact between two single-band superconductors.

those of the junction between single-band superconductors, see Fig. 2). The $I(\chi)$ dependence is, according to Eq. (7), as follows:

$$I = \frac{\pi |\Delta|}{e R_{N1}} \sin \frac{\chi}{2} \text{sgn} \cos \frac{\chi}{2} - \frac{\pi |\Delta|}{e R_{N2}} \cos \frac{\chi}{2} \text{sgn} \sin \frac{\chi}{2}, \quad (11)$$

and the energy of the Josephson junction, according to Eq. (8), is equal to

$$E = - \frac{\Phi_0 |\Delta|}{2e R_{N1}} \left| \cos \frac{\chi}{2} \right| - \frac{\Phi_0 |\Delta|}{2e R_{N2}} \left| \sin \frac{\chi}{2} \right|. \quad (12)$$

Several conclusions follow from Eqs. (11) and (12). First, the Josephson junction becomes frustrated (Fig. 3) with two-fold degenerate ground state

$$X^{(1)} = 2 \arctan \left(\frac{R_{N1}}{R_{N2}} \right) \quad \text{and} \quad X^{(2)} = 2\pi - \arctan \left(\frac{R_{N1}}{R_{N2}} \right). \quad (13)$$

Secondly, the frustrated ground state corresponds to a non-zero phase difference (normal contact, see Fig. 2) or π (π -contact). Following the definition of Ref. 35, we call such a Josephson system φ -contact. Thus, the Josephson system formed by a conventional and a two-band superconductor with the s_{\pm} -wave symmetry of the order parameter leads to a frustrated φ -contact. Note that the possibility of a frustrated tunnel junction between a single-band and a two-band s_{\pm} superconductor has already been predicted in the phenomenological Ginzburg-Landau theory.³⁶

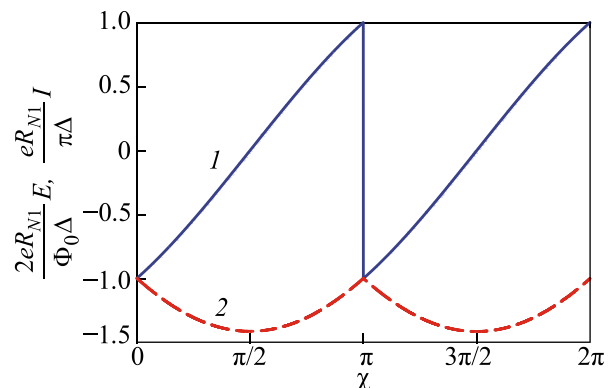


FIG. 3. Current-phase dependence (blue, I) and the Josephson energy (red, 2) of a point contact between a single-band and a two-band superconductor with the s_{\pm} -wave symmetry of the order parameter. The ratio $R_{N1}/R_{N2} = 1$.

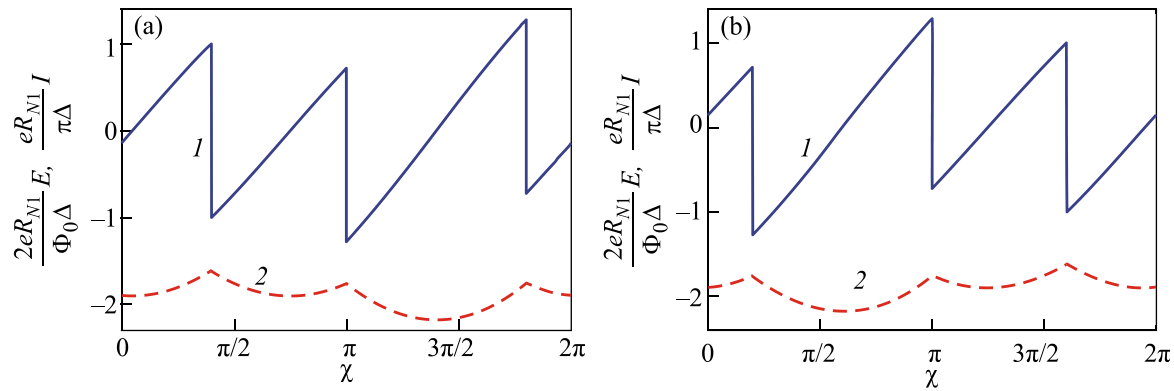


FIG. 4. Current-phase dependence (blue, I) and the Josephson energy (red, 2) of a point contact between a single-band and a three-band superconductor with time-reversal symmetry breaking and frustrated ground states (a) $\varphi = 0.6\pi$ and $\theta = 1.2\pi$ and (b) $\varphi = 1.4\pi$ and $\theta = 0.8\pi$.

The behavior of the Josephson junction, which is formed by a single-band and a three-band superconductor, is much more complicated. First of all, this is due to the presence of time-reversal symmetry breaking in the three-band superconductor, which leads to frustration—the emergence of two ground states in the bulk three-band superconductor, $\varphi_2 = \varphi$ and $\varphi_3 = \theta$. In this case, the phase differences are determined by Eqs. (3)–(6). According to Eq. (7), the Josephson current through the junction is defined as

$$I = \frac{\pi|\Delta|}{eR_{N1}} \sin \frac{\chi}{2} \operatorname{sgn} \cos \frac{\chi}{2} + \frac{\pi|\Delta|}{eR_{N2}} \sin \frac{\chi + \phi}{2} \operatorname{sgn} \cos \frac{\chi + \phi}{2} + \frac{\pi|\Delta|}{eR_{N3}} \sin \frac{\chi + \theta}{2} \operatorname{sgn} \cos \frac{\chi + \theta}{2}, \quad (14)$$

and the Josephson energy is, according to Eq. (8),

$$E = -\frac{\Phi_0|\Delta|}{2eR_{N1}} \left| \cos \frac{\chi}{2} \right| - \frac{\Phi_0|\Delta|}{2eR_{N2}} \left| \cos \frac{\chi + \phi}{2} \right| - \left| \cos \frac{\chi + \theta}{2} \right|. \quad (15)$$

To investigate the properties and characteristics of the Josephson junction, the phase differences φ and θ can be chosen arbitrarily since it is always possible to select such values of the coupling constants λ_{ij} , that satisfy Eqs. (2)–(6). In other words, after φ and θ are selected, there are five equations and two inequalities to determine nine coupling constants. Three of the equations are consistency equations (3)–(6), two others result from the respective equations determining phase differences φ and θ , and two inequalities

follow from the second variation of the energy of a bulk three-band superconductor, which determine the stability of the ground states of the bulk three-band superconductor.

Using these arguments, let us consider a three-band superconductor with time-reversal symmetry breaking by selecting one of the ground states in the form $\varphi = 0.6\pi$ and $\theta = 1.2\pi$. Since the above phase differences are in the second and third quadrants, respectively, they belong to the intervals $\varphi \in [\pi/2, 3\pi/2]$ and $\theta \in [\pi/2, 3\pi/2]$, and the other ground state corresponds to $\varphi = 1.4\pi$ and $\theta = 0.8\pi$.

The dependences of the energy and current on the phase difference across the Josephson junction are shown in Fig. 4.

As can be seen, the frustration of the ground state of a bulk three-band superconductor gives rise to two different dependences $I(\chi)$ and $E(\chi)$. Practically, this means that in a set of experimental measurements, various current-phase characteristics of the Josephson junction can be observed. Which of them is realized in the specific experiment depends on the history of the three-band superconductor, i.e., in which of the frustrated states is the three-band superconductor during this measurement.

Moreover, the dependence $E(\chi)$ clearly indicates that the Josephson system with a three-band superconductor in the frustrated state with $\varphi = 0.6\pi$ and $\theta = 1.2\pi$ or $\varphi = 1.4\pi$ and $\theta = 0.8\pi$ behaves like a φ -junction. We also found that such a ballistic junction formed by a single-band and three-band superconductor with time-reversal symmetry breaking has, in addition to the global minimum, two local minima in the dependence $E(\chi)$ (Fig. 4).

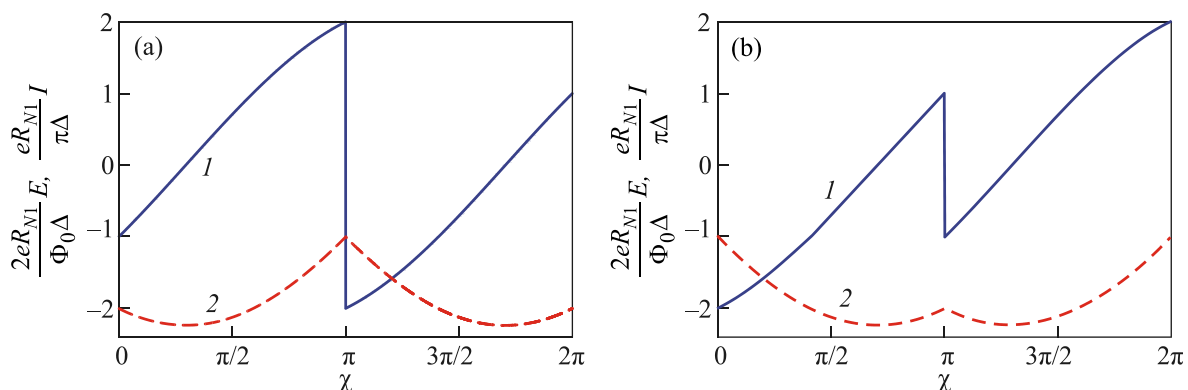


FIG. 5. Current-phase dependence (blue, I) and the Josephson energy (red, 2) of a point contact between a single-band and a three-band superconductor without time-reversal symmetry breaking and ground states (a) $\varphi = 0$ and $\theta = \pi$ and (b) $\varphi = \pi$ and $\theta = \pi$.

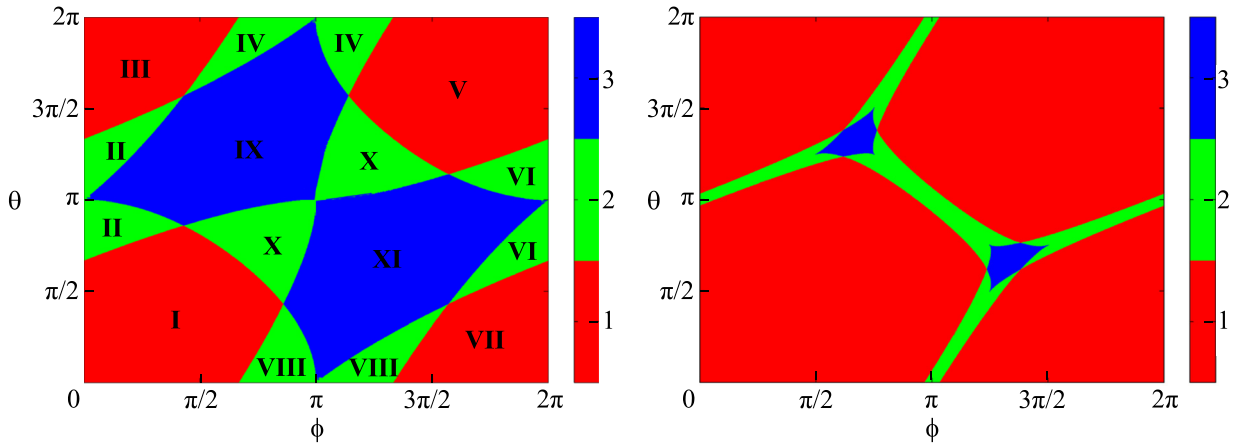


FIG. 6. Dependence of the total number (global and local) of energy minima of a ballistic (left) and a diffusive (right) Josephson junction formed by a single-band and a three-band superconductor on the parameters of the ground state (ϕ and θ) of the latter.

We now consider the properties of the Josephson junction, which is formed by a single-band and a three-band superconductor without breaking the time-reversal symmetry which has the ground states $\varphi = 0$ and $\theta = \pi$ or $\varphi = \pi$ and $\theta = \pi$ (the case $\varphi = 0, \theta = 0$ is trivial and qualitatively matches the properties of a Josephson junction formed by single-band superconductors). Current-phase dependences and the energy of the Josephson junction are shown in Fig. 5. In spite of the absence of degeneracy of the ground state of a bulk three-band superconductor, the Josephson junction is frustrated and exhibits signs of φ -contact.

Based on Eqs. (14) and (15), we constructed a phase diagram for the Josephson junction between single-band and three-band superconductors, which shows the total number of energy minima of the system depending on the position of the ground state of the bulk three-band superconductor (Fig. 6, left).

As can be seen, the phase diagram is divided into sectors according to the number of energy minima of the Josephson junction. Depending on the values of φ and θ , the number of minima changes from one to three. For each of the eleven sectors (I–XI), the position of the minima is given by the expressions in Appendix A. However, the most notable feature of the ballistic junction formed by single-band and three-band superconductors is much wider variety of the states of the Josephson junction in comparison with a similar system in the dirty limit (Fig. 6, right). In other words, for the Josephson junction with diffusive conductivity the intervals in which several energy minima exist are significantly narrower (see Appendix B).

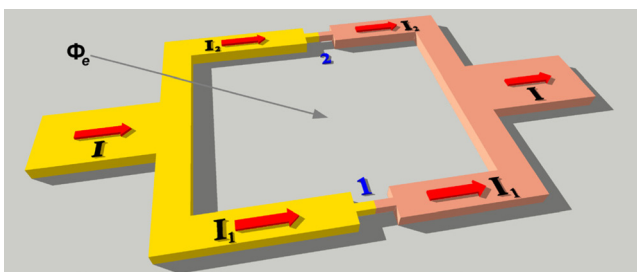


FIG. 7. Schematics of a dc SQUID containing Josephson point contacts between a single-band (coral color) and a multi-band (yellow) superconductor with an applied current I and magnetic flux Φ_e . I_1 and I_2 denote the respective currents in point contacts 1 and 2 of the dc SQUID.

4. Behavior of a dc SQUID based on the Josephson point contacts between single- and multi-band superconductors

It is well known that if one or more Josephson junctions are placed into a superconducting ring, there arise a number of novel features related to macroscopic quantum interference. This section will explore these phenomena in a dc SQUID—a system consisting of two point contacts linked by s -wave single- and multi-band superconductors (Fig. 7).

Following the above notation, we denote the junction phase difference between the first order parameter of the multi-band superconductor and the order parameter of the single-band superconductor as χ_i , where $i = 1, 2$ is the contact number. The uniqueness of the phase difference along the contour, the thickness of which is greater than the London penetration depth for both single-band and multi-band superconductors, requires the following condition to be fulfilled

$$(\chi_1 + \phi_i) - (\chi_2 + \phi_i) = 2\pi \frac{\Phi}{\Phi_0}, \quad (16)$$

where Φ is the total magnetic flux through the system and Φ_0 is the magnetic flux quantum. Recall that φ_i denotes the phase difference between the i -th and the first order parameters of the n -band superconductor and defines its ground states.

Quantization condition (16) should be supplemented by the first Kirchhoff's law and the condition for the total magnetic flux

$$I = I_1 + I_2, \quad (17)$$

$$\Phi = \Phi_e + L_1 I_1 - L_2 I_2, \quad (18)$$

where I_1 and I_2 are the currents flowing through the contacts, Φ_e is the external magnetic flux, L_1 and L_2 are the inductances of each arm of the dc SQUID. These inductances can be represented as $L_1 = \alpha L$ and $L_2 = (1 - \alpha)L$, where L is the total inductance of the SQUID ring.³⁷

Using condition (16), Eqs. (4) and (5) can be rewritten in the dimensionless form:

$$i_1 = (1 - \alpha)i + \frac{1}{\beta_{L1}} [(\chi_1 - \chi_2) - \chi_e], \quad (19)$$

$$i_2 = \alpha i - \frac{1}{\beta_{L1}} [(\chi_1 - \chi_2) - \chi_e], \quad (20)$$

where the currents i , i_1 and i_2 are now expressed in units of the first-band critical current of the multiband superconductor with no account taken of the interband interactions for the first point junction $I_{c1}^{(1)}$, the main parameter of the SQUID has the form $\beta_{L1} = (2\pi L I_{c1}^{(1)})/\Phi_0$ and external flux $\chi_e = (2\pi\Phi_e)/\Phi_0$.

After introduction of dimensionless variables, the currents i_1 and i_2 can be expressed as

$$i_j = \sum_i \frac{R_{N1}^{(1)}}{R_{Ni}^{(j)}} \sin \frac{\chi_j + \phi_i \text{sgn}(i-1)}{2} \times \text{sgn} \left(\cos \frac{\chi_j + \phi_i \text{sgn}(i-1)}{2} \right), \quad (21)$$

where $R_{Ni}^{(j)}$ are the partial contributions of each band of the multi-band superconductor to the normal resistance of the j -th contact.

Equations (19) and (20) can be obtained from the variation of the energy E with the variables χ_j :

$$E(\chi_1, \chi_2) = \frac{1}{2\beta_{L1}} [(\chi_2 - \chi_1) + \chi_e]^2 - i[(1 - \alpha)\chi_1 + \alpha\chi_2] + E_J(\chi_1, \chi_2). \quad (22)$$

Here $E_J(\chi_1, \chi_2)$ is an expression for the total Josephson energy of the dc SQUID point contacts

$$E_J(\chi_1, \chi_2) = - \sum_j \sum_i \frac{R_{N1}^{(1)}}{R_{Ni}^{(j)}} \left| \cos \frac{\chi_j + \phi_i \text{sgn}(i-1)}{2} \right|, \quad (23)$$

which follows from Eq. (8).

Let us begin the study of the dc SQUID behavior by considering its energy as a function of the phase difference at the contacts χ_2 and χ_1 , which depends on the magnitude of the applied magnetic flux. Unless otherwise stated, for the sake of simplicity in the following we will consider a symmetric dc SQUID with identical point contacts $R_{N1}^{(1)}/R_{Ni}^{(j)} = 1$.

Fig. 8 shows the contour plots of the surface $E(\chi_1, \chi_2)$ for dc SQUIDs with Josephson junctions formed between two single-band superconductors (Figs. 8(a) and 8(b)), single-band and s_{\pm} dual-band superconductors (Figs. 8(c) and 8(d)), single-band and three-band superconductors with violation of the time-reversal symmetry (Figs. 8(e) and 8(f)), and between one-band and three-band superconductors without breaking the time-reversal symmetry (Figs. 8(g)–8(j)) for zero magnetic flux (left column in Fig. 8) and the magnetic flux corresponding to the half flux quantum (right column in Fig. 8).

In the case of a dc SQUID based on a two-band superconductor with the s_{\pm} -wave symmetry of the order parameter, the energy minimum is degenerate at zero magnetic flux Φ_e (Fig. 8(c)) due to the frustration of the Josephson junction (see Fig. 3). For the same reason (see Figs. 5(a) and 5(b)), a degeneracy occurs for a three-band superconductor without time-reversal symmetry breaking (Figs. 8(d) and 8(g)).

In a magnetic field ($\Phi_e = \Phi_0/2$), dc SQUIDs based on an s_{\pm} two-band and three-band superconductors without time-reversal symmetry breaking (Figs. 8(d), 8(f), and 8(h), respectively) exhibit qualitatively the same behavior as a

normal dc SQUID based on single-band superconductors (Fig. 8(b)).

The most interesting features emerge for a dc SQUID based on a three-band superconductor with time-reversal symmetry breaking. At zero magnetic flux, there is only a shift of the position of the global energy minimum of the dc SQUID from the zero point $\chi_1 = \chi_2 = 0$ (Fig. 8(i)) despite the presence of time-reversal symmetry breaking in the bulk three-band superconductor. However at $\Phi_e = \Phi_0/2$, due to time-reversal symmetry breaking, a unique feature emerges—a strong degeneration of the energy minimum (Fig. 8(a)), which is not realized in other dc SQUIDs based on single-band or multiband superconductors without time-reversal symmetry breaking (Figs. 8(b), 8(d), 8(f), and 8(h)). Figs. 8(i) and 8(k) are contour plots of the energy of a dc SQUID based on a three-band superconductor with the ground state $\varphi = 0.6\pi$ and $\theta = 1.2\pi$. For a three-band superconductor in another ground state, $\varphi = 1.4\pi$ and $\theta = 0.8\pi$, the above behavior remains qualitatively the same, differing only in a symmetrical arrangement of the minima for $\Phi_e = \Phi_0/2$ with respect to the line $\chi_1 - \chi_2 = \pi$.

One of the most important characteristics of a SQUID is the dependence of the critical current i_c on the external magnetic flux Φ_e . To simplify the analysis of this problem, it is commonly assumed that the inductance of the circuit is negligible, so that the net magnetic flux through the SQUID is equal to the external flux

$$\chi_1 - \chi_2 = 2\pi \frac{\Phi_e}{\Phi_0}. \quad (24)$$

In this case, the problem of finding the function $i_c = i_c(\Phi_e/\Phi_0)$ is equivalent to the problem of determining the maximum of the function

$$i(\chi_1, \chi_2) = i_1(\chi_1) + i_2(\chi_2), \quad (25)$$

taking into account the quantization condition, Eq. (16). Here, $i_1(\chi_1)$ and $i_2(\chi_2)$ are the dimensionless current-phase dependences defined by Eq. (21).

The dependence of the critical current on the external magnetic flux for a dc SQUID was sought numerically. This dependence for a dc SQUID based on the Josephson point contacts between single-band superconductors is plotted in Fig. 9(a). In what follows the critical current is normalized to its maximum value.

For a two-band superconductor with s_{++} -wave symmetry of the order parameter, the dependence $i_c = i_c(\Phi_e/\Phi_0)$ qualitatively agrees with the similar characteristic for a dc SQUID based on single-band superconductors (see Fig. 9(a)). Features emerge when the two-band superconductor has the s_{\pm} -wave type of symmetry (Fig. 9(b)). It can be seen that the critical current exhibit a saw-tooth behavior with the period $\Phi_0/2$ as opposed to the sinusoidal modulation with a period of one magnetic flux quantum in the case of a conventional single-band or a two-band superconductor with the s_{++} symmetry.

In the case of a three-band superconductor with time-reversal symmetry breaking, it was found that, despite the presence of two different possible current-phase relations,¹⁷ the dependence $i_c = i_c(\Phi_e/\Phi_0)$ is the same for both ground states of a bulk three-band superconductor (Fig. 9(c)). A similar situation occurs for a three-zone superconductor without time-reversal symmetry breaking, which has the

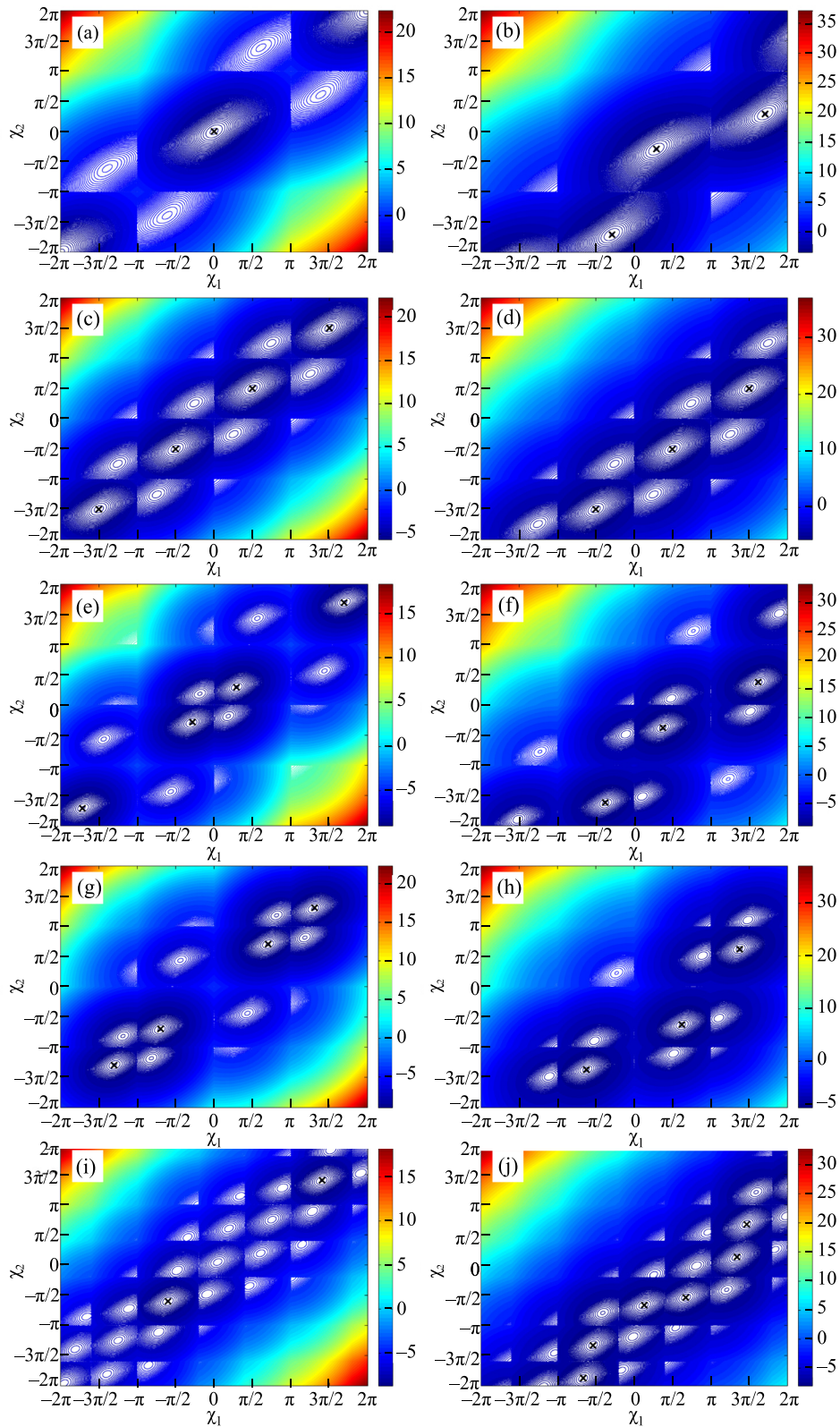


FIG. 8. Contour plot of the energy surface of a dc SQUID for zero external magnetic flux $\chi_e = 0$ ($\Phi/\Phi_0 = 0$, left column) and $\chi_e = \pi$ ($\Phi/\Phi_0 = 0.5$, right column) in the absence of transport current: (a) and (b) the point contacts between s -wave single-band superconductors; (c) and (d) the point contact between a single-band and a two-band superconductor with the s_{\pm} -wave symmetry of the order parameter; (e) and (f) and (g) and (h) the point contact between a single-band and a three-band superconductor without time-reversal symmetry breaking and the ground states $\varphi = 0, \theta = \pi$, and $\varphi = \pi, \theta = \pi$, respectively; (i) and (j) the point contact between a single-band and a three-band superconductor with time-reversal symmetry breaking in one of the frustrated ground states $\varphi = 0.6\pi$ and $\theta = 1.2\pi$ (the graph for another ground state $\varphi = 1.4\pi$ and $\theta = 0.8\pi$ is symmetric with respect to the line $\chi_1 - \chi_2 = \pi$). Crosses indicate the positions of the global minima. For all the SQUIDs, $\beta_{L1} = 3$.

ground states with the phases $\varphi = 0$ and $\theta = \pi$ and $\varphi = \pi$ and $\theta = \pi$ (Fig. 9(d)).

Comparing Figs. 9(c) and 9(d), we can conclude that the critical current for a three-band superconductor with time-

reversal symmetry breaking has a more complex structure with some additional peaks present in the dependence $i_c = i_c(\Phi_e/\Phi_0)$.

The introduction of asymmetry of the critical currents of the Josephson point contacts in a dc SQUID naturally leads to

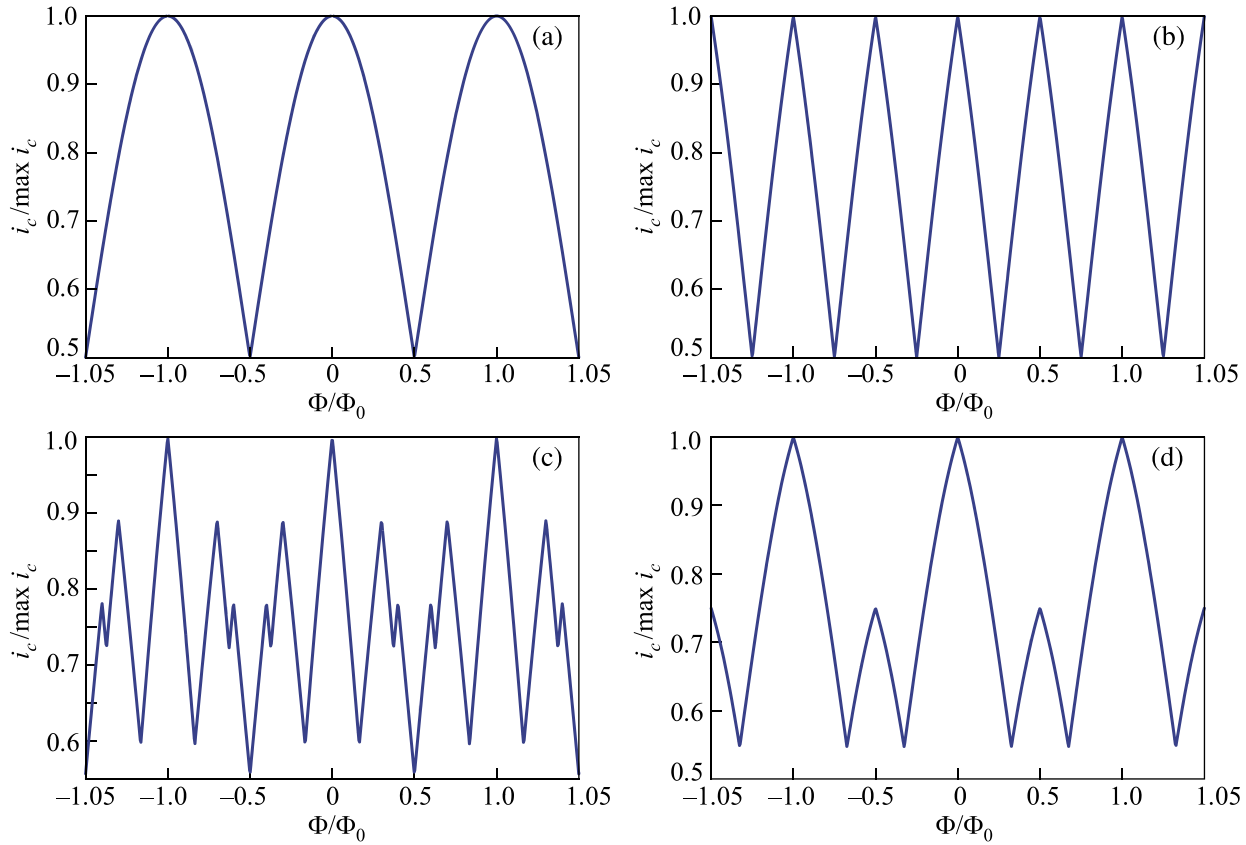


FIG. 9. Dependences of the critical current of a symmetric dc SQUID with negligible inductance on the applied magnetic flux for (a) single-band superconductor, (b) two-band superconductor with the s_{\pm} -wave symmetry of the order parameter, (c) three-band superconductor with time-reversal symmetry breaking and frustrated ground states $\varphi = 0.6\pi$ and $\theta = 1.2\pi$ and $\varphi = 1.4\pi$ and $\theta = 0.8\pi$, (d) three-band superconductor without time-reversal symmetry breaking and ground states $\varphi = 0$ and $\theta = \pi$ and $\varphi = \pi$ and $\theta = \pi$.

an asymmetry of the critical current dependence on the external magnetic flux (Fig. 10). This effect is particularly noticeable in a three-band superconductor both with time-reversal symmetry breaking (Fig. 10(c)) and without it (Fig. 10(d)).

Let us now consider the S -states of a dc SQUID, i.e., the dependences of the net magnetic flux through the loop on the external magnetic flux in the case of no transport current $i = 0$. Assuming the critical currents of the junctions equal, the dc SQUID can be replaced with the equivalent circuit containing an rf SQUID with a phase difference at the contact χ_{rf} . This phase difference is related to the phase differences χ_1 and χ_2 of the dc SQUID through the relations

$$\chi_1 = \Delta\chi + \chi_{rf}, \quad (26)$$

$$\chi_2 = \Delta\chi - \chi_{rf}, \quad (27)$$

where $\Delta\chi$ is a certain parameter which can be obtained by summing Eqs. (19) and (20) and taking into account the form of the current-phase relation (21)

$$\sum_j \sum_i \sin \frac{\chi_j + \phi_i \text{sgn}(i-1)}{2} \times \text{sgn} \left(\cos \frac{\chi_j + \phi_i \text{sgn}(i-1)}{2} \right) = 0 \quad (28)$$

and Eqs. (26) and (27) for the new variable χ_{rf} .

The magnitude of the parameter $\Delta\chi$ depends on what superconductors are in contact in the dc SQUID. If the dc SQUID is formed by the Josephson junctions between

single-band superconductors, then in the interval $\Delta\chi \in [0, 2\pi)$, this parameter is

$$\Delta\chi = 0 \quad \text{and} \quad \Delta\chi = \pi. \quad (29)$$

For a system of junctions between a single-band and a two-band superconductor with s_{\pm} -wave symmetry of the order parameter

$$\Delta\chi = 0, \quad \Delta\chi = \frac{\pi}{2}, \quad \Delta\chi = \pi \quad \text{and} \quad \Delta\chi = \frac{3\pi}{2}. \quad (30)$$

For a three-band superconductor, the parameter $\Delta\chi$ depends on φ and θ , which, as well known, define the ground states of the bulk three-band superconductor. In this case, $\Delta\chi$ can be found only by numerical solution of Eqs. (26)–(28). The exception is the case of a three-band superconductor without time-reversal symmetry breaking, since its $\Delta\chi$ parameter is the same as for a dc SQUID based on single-band superconductors, Eq. (29).

Given the variable substitution (26) and (27), Eqs. (19) and (20) are converted into

$$\chi_{rf} + \frac{1}{2} \beta_{L1} \sum_i \sin \frac{\chi_{rf} + \Delta\chi + \phi_i \text{sgn}(i-1)}{2} \times \text{sgn} \left(\cos \frac{\chi_{rf} + \Delta\chi + \phi_i \text{sgn}(i-1)}{2} \right) = \frac{1}{2} \chi_e. \quad (31)$$

This equation is transcendental, thus its solutions (the number of the solutions is equal to the number of possible values of the parameter $\Delta\chi$ in the range $\Delta\chi \in [0, 2\pi)$, see

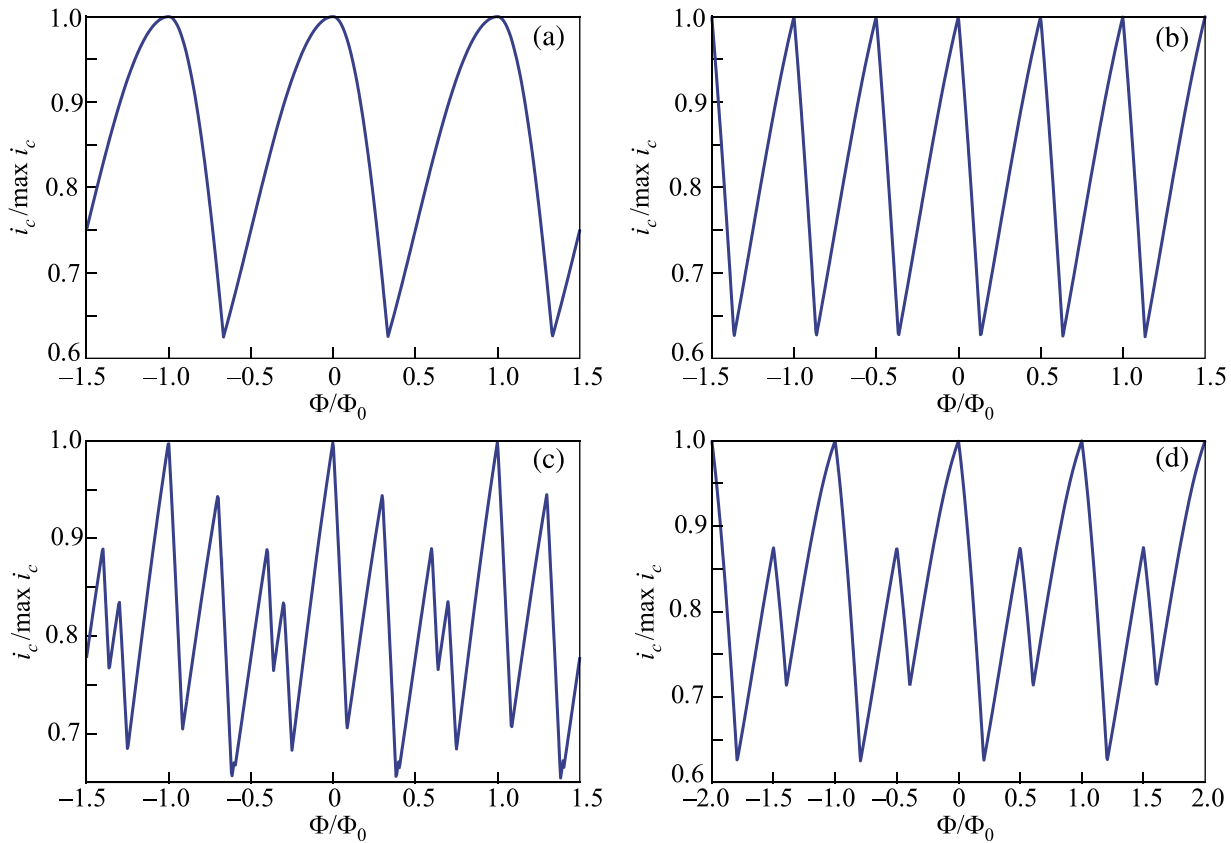


FIG. 10. Dependence of the critical current of an asymmetric ($R_{N1}^{(1)}/R_{N1}^{(2)} = 1$ and $R_{N1}^{(1)}/R_{N1}^{(2)} = 3$) dc SQUID with negligible inductance on the magnetic flux applied for (a) single-band superconductor, (b) two-band superconductor with the s_{\pm} -wave symmetry of the order parameter, (c) three-band superconductor with time-reversal symmetry breaking and frustrated ground states $\varphi = 0.6\pi$ and $\theta = 1.2\pi$ and $\varphi = 1.4\pi$ and $\theta = 0.8\pi$, (d) three-band superconductor without time-reversal symmetry breaking and ground states $\varphi = 0$ and $\theta = \pi$ and $\varphi = \pi$ and $\theta = \pi$.

above)—the functions $\chi_{rf}(\chi_e)$ —can be found only numerically. Knowing the dependence $\chi_{rf}(\chi_e)$ and taking into account Eqs. (26) and (27), we can find the S -states of a dc SQUID consisting of the Josephson junctions between two single-band superconductors (Fig. 11(a)), a single-band and a two-band s_{\pm} -wave superconductor (Fig. 11(b)), a single-band and a three-band superconductor with time-reversal symmetry breaking (Fig. 11(c)), and a single-band and a three-band superconductor without time-reversal symmetry breaking (Fig. 11(d)).

Let us make few comments regarding the S -states of a dc SQUID presented in Fig. 11. The figure does not show the dependences $\Phi(\Phi_e)$ for a two-band s_{++} -superconductor and a three-band superconductor with the ground state $\varphi = \theta = 0$, since they qualitatively match the respective characteristics of a single-band superconductor (Fig. 11(a)), differing only quantitatively. Despite the fact that Eq. (31) has four solutions for a two-band s_{\pm} -wave superconductor, the S -states for $\Delta\chi = 0$ and $\Delta\chi = \pi$ coincide with each other (solid line in Fig. 11(b)). The same is true for the states $\Delta\chi = \pi/2$ and $\Delta\chi = 3\pi/2$ (dashed line in Fig. 11(b)).

A similar situation occurs for a dc SQUID based on a three-band superconductor with time-reversal symmetry breaking. Figure 11(c) shows the S -states for a three-band superconductor with the frustrated ground states $\varphi = 0.6\pi$ and $\theta = 1.2\pi$ and $\varphi = 1.4\pi$ and $\theta = 0.8\pi$. Evidently, in this case, four different $\Phi(\Phi_e)$ dependences are possible, however, for example, for $\varphi = 0.6\pi$ and $\theta = 1.2\pi$, the S -states with the respective parameters $\Delta\chi = 1.25664$ and $\Delta\chi = 1.25664 + \pi$ coincide pairwise with the S -states arising at $\varphi = 1.4\pi$ and $\theta = 0.8\pi$ with the parameters $\Delta\chi = 2\pi -$

1.25664 and $\Delta\chi = \pi - 1.25664$. The same pattern can be implemented for other three-band superconductors with broken time-reversal symmetry.

For a three-band superconductor without time-reversal symmetry breaking, the S -states for $\varphi = 0$ and $\theta = \pi$ with the parameters $\Delta\chi = 0$ and $\Delta\chi = \pi$ (Fig. 11(d)) are identical to the S -states for $\varphi = \pi$, $\theta = \pi$ with the parameters $\Delta\chi = \pi$ and $\Delta\chi = 0$, respectively.

As in the case of a dc SQUID based on single-band superconductors, the S -states are stable only if the derivative $d\Phi/d\Phi_e > 0$. In other words, the S -states are stable in the intervals where $\Phi(\Phi_e)$ dependences have a positive slope.

In comparison with the hysteretic behavior of dc SQUIDs based on single-band superconductors (Fig. 11(a)), the S -states of dc SQUIDs based on multi-band superconductors can demonstrate a multi-hysteresis behavior. Moreover, the greater is the number of energy gaps, the more jumps can be detected when measuring the $\Phi(\Phi_e)$ dependence. As Fig. 11(c) implies, the largest number of hysteresis loops can be observed in a three-band superconductor with time-reversal symmetry breaking. Therefore, the presence of the S -states in a dc SQUID can be regarded as a kind of necessary condition for the possible existence of multi-bands in the superconducting compound and realization of time-reversal symmetry breaking.

5. Conclusion

In summary, we have studied the properties of Josephson systems based on point contacts with ballistic

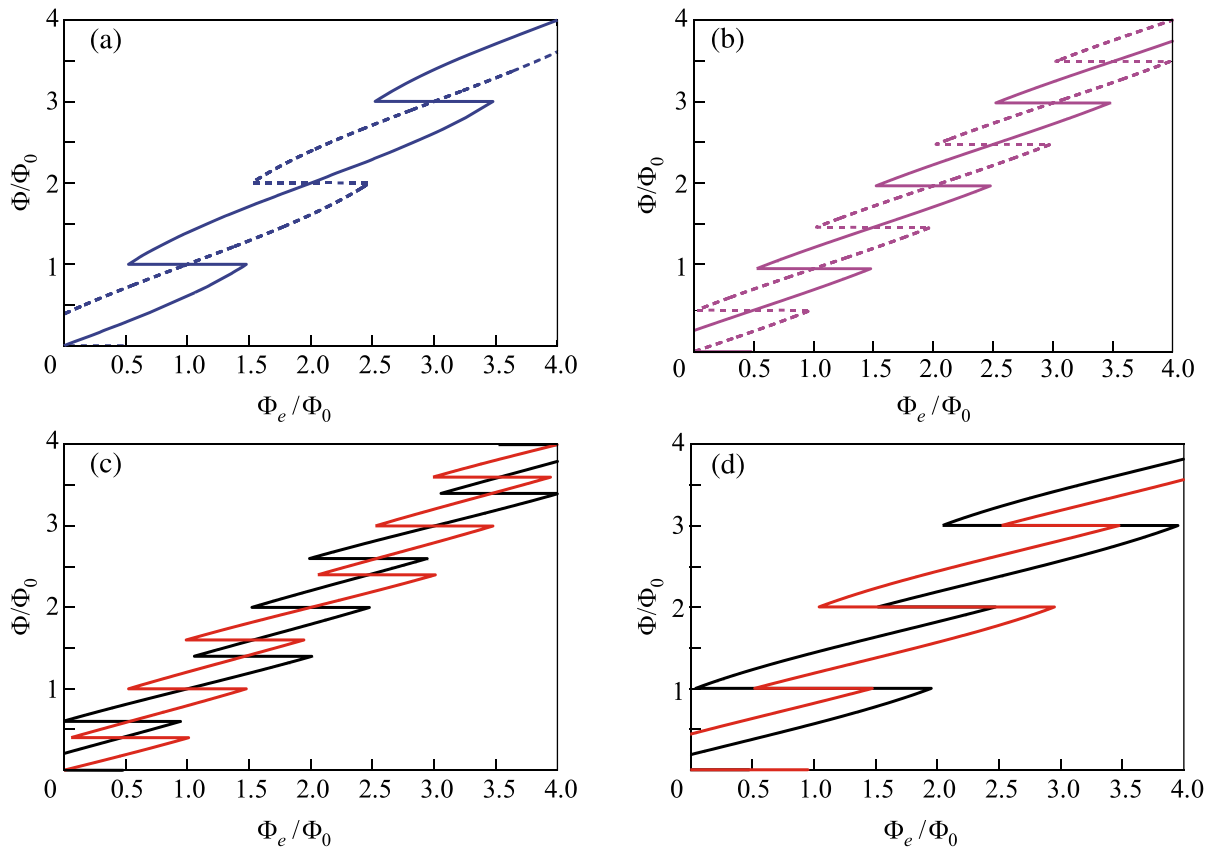


FIG. 11. S -states in a dc SQUID based on the Josephson junctions between (a) single-band superconductors, (b) a single-band and a two-band s_{\pm} -wave superconductor, (c) a single-band and a three-band superconductor with time-reversal symmetry breaking, (d) a single-band and a three-band superconductor without time-reversal symmetry breaking. In the case of a three-band superconductor with time-reversal symmetry breaking, the S -states correspond to the ground state $\varphi = 0.6\pi$ and $\theta = 1.2\pi$ with the parameter $\Delta\chi = 1.25664$ (black line) and $\varphi = 1.4\pi$ and $\theta = 0.8\pi$ with the parameter $\Delta\chi = \pi - 1.25664$ (red line). In the case of a three-band superconductor without time-reversal symmetry breaking, the S -states correspond to the ground states $\varphi = 0$ and $\theta = \pi$ with the parameter $\Delta\chi = 0$ (black line) and $\varphi = \pi$ and $\theta = \pi$ with $\Delta\chi = 0$ (red line). The solid and dotted lines in the panels (a) and (b) show two possible S -states of a conventional dc SQUID. The reason for the absence of the dotted lines for a three-band superconductor is explained in the main text. For all dependences $\beta_{L1} = 3$.

conduction formed between a single-band and a multi-band (two- and three-band) superconductor at zero temperature. The ballistic Josephson point contact between a single-band and an s_{\pm} -wave superconductor is frustrated, has two ground states, and thus demonstrates the properties of a φ -contact. If the Josephson junction is formed by a single-band and a three-band superconductor with time-reversal symmetry breaking, such a contact may have two different current-phase characteristics, also demonstrating the φ -contact properties. Furthermore, depending on the ground state of the three-band superconductor with time-reversal symmetry breaking, the actual Josephson junction can have from one to three energy minima. These minima can be either all stable in the global sense (three-fold degeneracy of the ground state) or only one of them can be globally stable. For a three-band superconductor, which is characterized by the absence of time-reversal symmetry breaking, the Josephson junction has qualitatively the same properties as the contact with an s_{\pm} -wave two-band superconductors, it is a frustrated (two-fold degenerate) φ -contact. It was established that in comparison with the Josephson junction with a diffusive contact, the ballistic junction between a single-band and a three-band superconductor can exhibit a significantly wider variety of states with additional local or global energy minima.

We also considered the behavior of a dc SQUID based on the studied Josephson junctions formed by a single-band and a multi-band superconductor. We found the differences in the characteristics of dc SQUIDs (the dependences of the critical current and the S -state) constructed of an s_{\pm} -wave superconductor, a three-band superconductor with time-reversal symmetry breaking and a three-band superconductor without time reversal symmetry breaking as compared with conventional dc SQUID based on single-band superconductors.

The above features can be used to detect the presence of a multi-band structure in superconductors. Moreover, in the case of a three-band superconductor these results can help to detect time-reversal symmetry breaking.

This work was supported by a grant from the State Agency of Ukraine on E-Governance (M/231-2013) and a grant from the German Federal Ministry of Education and Research (UKR-2012-028). One of the authors (Y.S.E.) was supported by a grant from the Russian Science Foundation No. 15-12-10020.

APPENDIX A

The phase diagram in Fig. 6(a) consists of 11 sectors, each of which corresponds to a certain number of energy minima of the ballistic Josephson junction formed by a

single-band and a three-band superconductor. The position of each minimum (local and/or global) is defined by the following equations:

Sector I (one minimum)

$$X^{(1)} = 2\pi - 2\text{arccot} \frac{1 + 2 \cos \frac{\phi + \theta}{4} \cos \frac{\phi - \theta}{4}}{2 \sin \frac{\phi + \theta}{4} \cos \frac{\phi - \theta}{4}}. \quad (\text{A1})$$

Sector II (two minima)

$$X^{(1)} = 2\pi - 2\text{arccot} \frac{1 + 2 \cos \frac{\phi + \theta}{4} \cos \frac{\phi - \theta}{4}}{2 \sin \frac{\phi + \theta}{4} \cos \frac{\phi - \theta}{4}}, \quad (\text{A2})$$

$$X^{(2)} = 2\text{arccot} \frac{1 + 2 \sin \frac{\theta + \phi}{4} \sin \frac{\theta - \phi}{4}}{2 \sin \frac{\theta - \phi}{4} \cos \frac{\theta + \phi}{4}}. \quad (\text{A3})$$

Sector III (one minimum)

$$X^{(1)} = \begin{cases} 2\text{arccot} \frac{1 + 2 \sin \frac{\theta + \phi}{4} \sin \frac{\theta - \phi}{4}}{2 \sin \frac{\theta - \phi}{4} \cos \frac{\theta + \phi}{4}}, & \phi + \theta < 2\pi \\ 2\pi + 2\text{arccot} \frac{1 + 2 \sin \frac{\theta + \phi}{4} \sin \frac{\theta - \phi}{4}}{2 \sin \frac{\theta - \phi}{4} \cos \frac{\theta + \phi}{4}}, & \phi + \theta > 2\pi, \end{cases} \quad (\text{A4})$$

Sector IV (two minima)

$$X^{(1)} = 2\pi + 2\text{arccot} \frac{1 - 2 \cos \frac{\phi + \theta}{4} \cos \frac{\phi - \theta}{4}}{2 \sin \frac{\phi + \theta}{4} \cos \frac{\phi - \theta}{4}}, \quad (\text{A5})$$

$$X^{(2)} = 2\text{arccot} \frac{1 + 2 \sin \frac{\theta + \phi}{4} \sin \frac{\theta - \phi}{4}}{2 \sin \frac{\theta - \phi}{4} \cos \frac{\theta + \phi}{4}}, \quad (\text{A6})$$

Sector V (one minimum)

$$X^{(1)} = 2\text{arccot} \frac{1 - 2 \cos \frac{\phi + \theta}{4} \cos \frac{\phi - \theta}{4}}{2 \sin \frac{\phi + \theta}{4} \cos \frac{\phi - \theta}{4}}, \quad (\text{A7})$$

Sector VI (two minima)

$$X^{(1)} = 2\text{arccot} \frac{1 - 2 \cos \frac{\phi + \theta}{4} \cos \frac{\phi - \theta}{4}}{2 \sin \frac{\phi + \theta}{4} \cos \frac{\phi - \theta}{4}}, \quad (\text{A8})$$

$$X^{(2)} = 2\pi + 2\text{arccot} \frac{-1 + 2 \sin \frac{\theta + \phi}{4} \sin \frac{\theta - \phi}{4}}{2 \sin \frac{\theta - \phi}{4} \cos \frac{\theta + \phi}{4}}, \quad (\text{A9})$$

Sector VII (one minimum)

$$X^{(1)} = \begin{cases} 2\text{arccot} \frac{-1 + 2 \sin \frac{\theta + \phi}{4} \sin \frac{\theta - \phi}{4}}{2 \sin \frac{\theta - \phi}{4} \cos \frac{\theta + \phi}{4}}, & \phi + \theta < 2\pi \\ 2\pi + 2\text{arccot} \frac{-1 + 2 \sin \frac{\theta + \phi}{4} \sin \frac{\theta - \phi}{4}}{2 \sin \frac{\theta - \phi}{4} \cos \frac{\theta + \phi}{4}}, & \phi + \theta > 2\pi \end{cases} \quad (\text{A10})$$

Sector VIII (two minima)

$$X^{(1)} = 2\pi - 2\text{arccot} \frac{1 + 2 \cos \frac{\phi + \theta}{4} \cos \frac{\phi - \theta}{4}}{2 \sin \frac{\phi + \theta}{4} \cos \frac{\phi - \theta}{4}}, \quad (\text{A11})$$

$$X^{(2)} = 2\text{arccot} \frac{-1 + 2 \sin \frac{\theta + \phi}{4} \sin \frac{\theta - \phi}{4}}{2 \sin \frac{\theta - \phi}{4} \cos \frac{\theta + \phi}{4}}, \quad (\text{A12})$$

Sector IX (three minima)

$$X^{(1)} = 2\pi - 2\text{arccot} \frac{1 + 2 \cos \frac{\phi + \theta}{4} \cos \frac{\phi - \theta}{4}}{2 \sin \frac{\phi + \theta}{4} \cos \frac{\phi - \theta}{4}}, \quad (\text{A13})$$

$$X^{(2)} = 2\text{arccot} \frac{1 - 2 \cos \frac{\phi + \theta}{4} \cos \frac{\phi - \theta}{4}}{2 \sin \frac{\phi + \theta}{4} \cos \frac{\phi - \theta}{4}}, \quad (\text{A14})$$

$$X^{(3)} = \begin{cases} 2\text{arccot} \frac{1 + 2 \sin \frac{\theta + \phi}{4} \sin \frac{\theta - \phi}{4}}{2 \sin \frac{\theta - \phi}{4} \cos \frac{\theta + \phi}{4}}, & \phi + \theta < 2\pi \\ 2\pi + 2\text{arccot} \frac{1 + 2 \sin \frac{\theta + \phi}{4} \sin \frac{\theta - \phi}{4}}{2 \sin \frac{\theta - \phi}{4} \cos \frac{\theta + \phi}{4}}, & \phi + \theta > 2\pi, \end{cases} \quad (\text{A15})$$

Sector X (two minima)

$$X^{(1)} = 2\pi - 2\text{arccot} \frac{1 + 2 \cos \frac{\phi + \theta}{4} \cos \frac{\phi - \theta}{4}}{2 \sin \frac{\phi + \theta}{4} \cos \frac{\phi - \theta}{4}}, \quad (\text{A16})$$

$$X^{(2)} = 2\text{arccot} \frac{1 - 2 \cos \frac{\phi + \theta}{4} \cos \frac{\phi - \theta}{4}}{2 \sin \frac{\phi + \theta}{4} \cos \frac{\phi - \theta}{4}}, \quad (\text{A17})$$

Sector XI (three minima)

$$X^{(1)} = 2\pi - 2\text{arccot} \frac{1 + 2 \cos \frac{\phi + \theta}{4} \cos \frac{\phi - \theta}{4}}{2 \sin \frac{\phi + \theta}{4} \cos \frac{\phi - \theta}{4}}, \quad (\text{A18})$$

$$X^{(2)} = 2\text{arccot} \frac{1 - 2 \cos \frac{\phi + \theta}{4} \cos \frac{\phi - \theta}{4}}{2 \sin \frac{\phi + \theta}{4} \cos \frac{\phi - \theta}{4}}, \quad (\text{A19})$$

$$X^{(3)} = \begin{cases} 2\text{arccot} \frac{-1 + 2 \sin \frac{\theta + \phi}{4} \sin \frac{\theta - \phi}{4}}{2 \sin \frac{\theta - \phi}{4} \cos \frac{\theta + \phi}{4}}, & \phi + \theta < 2\pi \\ 2\pi + 2\text{arccot} \frac{-1 + 2 \sin \frac{\theta + \phi}{4} \sin \frac{\theta - \phi}{4}}{2 \sin \frac{\theta - \phi}{4} \cos \frac{\theta + \phi}{4}}, & \phi + \theta > 2\pi, \end{cases} \quad (\text{A20})$$

APPENDIX B

The current-phase relation $I(\chi)$ and the energy of the Josephson junction $E(\chi)$ formed by a single-band and a three-band superconductor in the dirty limit is given by³²

$$I = \frac{\pi|\Delta|}{eR_{N1}} \cos \frac{\chi}{2} \text{artanh} \sin \frac{\chi}{2} + \frac{\pi|\Delta|}{eR_{N2}} \cos \frac{\chi + \phi}{2} \text{artanh} \sin \frac{\chi + \phi}{2} + \frac{\pi|\Delta|}{eR_{N3}} \cos \frac{\chi + \theta}{2} \text{artanh} \sin \frac{\chi + \theta}{2}, \quad (\text{B1})$$

$$E = \frac{|\Delta|\Phi_0}{2eR_{N1}} \left(2 \sin \frac{\chi}{2} \text{artanh} \sin \frac{\chi}{2} + \ln \cos^2 \frac{\chi}{2} \right) + \frac{|\Delta|\Phi_0}{2eR_{N2}} \left(2 \sin \frac{\chi + \phi}{2} \text{artanh} \sin \frac{\chi + \phi}{2} + \ln \cos^2 \frac{\chi + \phi}{2} \right) + \frac{|\Delta|\Phi_0}{2eR_{N3}} \left(2 \sin \frac{\chi + \theta}{2} \text{artanh} \sin \frac{\chi + \theta}{2} + \ln \cos^2 \frac{\chi + \theta}{2} \right), \quad (\text{B2})$$

where θ and ϕ define the ground state of a bulk three-band superconductor.

The phase diagram in Fig. 6 (right), which shows the number of ground states of the diffusive Josephson junction as a function of ϕ and θ , is based on Eqs. (B1) and (B2).

^{a)}Email: yuriyyerin@gmail.com

¹D. A. Wollman, D. J. Van Harlingen, W. C. Lee, D. M. Ginsberg, and A. J. Leggett, *Phys. Rev. Lett.* **71**, 2134 (1993).

²P. V. Komissinski, E. Il'ichev, G. A. Ovsyannikov, S. A. Kovtonyuk, M. Grajcar, R. Hlubina, Z. Ivanov, Y. Tanaka, N. Yoshida, and S. Kashiwaya, *Europhys. Lett.* **57**, 585 (2002).

³C. C. Tsuei and J. R. Kirtley, *Rev. Mod. Phys.* **72**, 969 (2000).

⁴Y. Kamihara, T. Watanabe, M. Hirano, and H. Hosono, *J. Am. Chem. Soc.* **130**, 3296 (2008).

⁵I. I. Mazin, D. J. Singh, M. D. Johannes, and M. H. Du, *Phys. Rev. Lett.* **101**, 057003 (2008).

⁶K. Kuroki, S. Onari, R. Arita, H. Usui, Y. Tanaka, H. Kontani, and H. Aoki, *Phys. Rev. Lett.* **101**, 087004 (2008).

⁷P. C. W. Chu et al., "Superconductivity in iron-pnictides," *Physica C* **469**(special issue), 313–674 (2009).

⁸J.-P. Paglione and R. L. Green, *Nat. Phys.* **6**, 645 (2010).

⁹B. Zeng, G. Mu, H. Q. Luo, T. Xiang, H. Yang, L. Shan, C. Ren, I. I. Mazin, P. C. Dai, and H.-H. Wen, *Nat. Commun.* **1**, 112 (2010).

¹⁰M. Tortello, D. Daghero, G. A. Ummarino, V. A. Stepanov, J. Jiang, J. D. Weiss, E. E. Hellstrom, and R. S. Gonnelli, *Phys. Rev. Lett.* **105**, 237002 (2010).

¹¹K. Okazaki, Y. Ito, Y. Ota, Y. Kotani, T. Shimojima, T. Kiss, S. Watanabe, C.-T. Chen, S. Niitaka, T. Hanaguri, H. Takagi, A. Chainani, and S. Shin, *Phys. Rev. Lett.* **109**, 237011 (2012).

¹²M. Abdel-Hafiez, V. Grinenko, S. Aswartham, I. Morozov, M. Roslov, O. Vakaliuk, S. Johnson, D. V. Efremov, J. van den Brink, H. Rosner, M. Kumar, C. Hess, S. Wurmehl, A. U. B. Wolter, B. Buechner, E. L. Green, J. Wosnitzer, P. Vogt, A. Reifemberger, C. Enss, M. Hempel, R. Klingeler, and S.-L. Drechsler, *Phys. Rev. B* **87**, 180507(R) (2013).

¹³V. Grinenko, D. V. Efremov, S.-L. Drechsler, S. Aswartham, D. Gruner, M. Roslova, I. Morozov, K. Nenkov, S. Wurmehl, A. U. B. Wolter, B. Holzapfel, and B. Büchner, *Phys. Rev. B* **89**, 060504(R) (2014).

¹⁴S. Johnston, M. Abdel-Hafiez, L. Harnagea, V. Grinenko, D. Bombor, Y. Krupskaya, C. Hess, S. Wurmehl, A. U. B. Wolter, B. Büchner, H. Rosner, and S.-L. Drechsler, *Phys. Rev. B* **89**, 134507 (2014).

¹⁵W.-C. Lee, S.-C. Zhang, and C. Wu, *Phys. Rev. Lett.* **102**, 217002 (2009).

¹⁶V. Stanev and A. E. Koshelev, *Phys. Rev. B* **89**, 100505(R) (2014).

¹⁷D. F. Agerberg, V. Barzykin, and L. P. Gor'kov, *Phys. Rev. B* **60**, 14868 (1999).

¹⁸V. Stanev and Z. Tesanovic, *Phys. Rev. B* **81**, 134522 (2010).

¹⁹Y. Tanaka and T. Yanagisawa, *J. Phys. Soc. Jpn.* **79**, 114706 (2010).

²⁰J. Carlstrom, J. Garaud, and E. Babaev, *Phys. Rev. B* **84**, 134518 (2011).

²¹R. G. Dias and A. M. Marques, *Supercond. Sci. Technol.* **24**, 085009 (2011).

²²T. Yanagisawa, Y. Takana, I. Hase, and K. Yamaji, *J. Phys. Soc. Jpn.* **81**, 024712 (2012).

²³X. Hu and Z. Wang, *Phys. Rev. B* **85**, 064516 (2012).

²⁴S. Z. Lin and X. Hu, *Phys. Rev. Lett.* **108**, 177005 (2012).

²⁵T. Bojesen, E. Babaev, and A. Sudbø, *Phys. Rev. B* **88**, 220511(R) (2013).

²⁶S. Maiti and A. V. Chubukov, *Phys. Rev. B* **87**, 144511 (2013).

²⁷S.-Z. Lin, *J. Phys.: Condens. Matter* **26**, 493202 (2014).

²⁸M. Mariani, L. Fanfarillo, C. Castellani, and L. Benfatto, *Phys. Rev. B* **88**, 214508 (2013).

²⁹J. Garaud and E. Babaev, *Phys. Rev. Lett.* **112**, 017003 (2014).

³⁰Y. S. Yerin, A. N. Omelyanchouk, and E. Il'ichev, *Supercond. Sci. Technol.* **28**, 095006 (2015).

³¹Y. Yerin, A. Omelyanchouk, S.-L. Drechsler, J. van den Brink, and D. V. Efremov (unpublished).

³²Y. S. Yerin and A. N. Omelyanchouk, *Fiz. Nizk. Temp.* **40**, 1206 (2014) [*Low Temp. Phys.* **40**, 943 (2014)].

³³I. O. Kulik and A. N. Omel'yanchuk, *Fiz. Nizk. Temp.* **4**, 296 (1978) [*Sov. J. Low Temp. Phys.* **4**, 142 (1978)].

³⁴I. O. Kulik and A. N. Omel'yanchuk, *Pis'ma Zh. Eksp. Teor. Fiz.* **21**, 216 (1975) [*JETP Lett.* **21**, 96 (1975)].

³⁵A. Buzdin and A. E. Koshelev, *Phys. Rev. B* **67**, 220504(R) (2003).

³⁶T. K. Ng and N. Nagaosa, *Eur. Phys. Lett.* **87**, 17003 (2009).

³⁷J. Clarke, W. M. Goubau, and M. B. Ketchen, *J. Low Temp. Phys.* **25**, 99 (1976).

Translated by L. Gardt